Graphene nanoribbon/graphene hybrid broadband infrared photodetectors

Shoichiro Fukushima, Masaaki Shimatani, and Shinpei Ogawa*
Mitsubishi Electric Corporation, Advanced Technology R&D Center, Amagasaki, Japan

Abstract. Graphene nanoribbons (GNRs) and graphene hybrid photodetectors were demonstrated in the middle- and long-wavelength infrared (MWIR and LWIR, respectively) regions. Graphene transistors were prepared using Si substrates with an SiO_2 layer and source and drain electrodes. Single-layer graphene fabricated by chemical vapor deposition was transferred onto the substrates to form a channel; the GNR was formed on this channel by solution dispersion. The formation of graphene and the GNR was confirmed by position mapping of the Raman spectra. The photoresponse was measured in the MWIR and LWIR regions, and was found to be drastically enhanced for devices with the GNR when compared with those without it. Although the devices without the GNR could not respond at temperatures higher than 15 K, those with the GNR could be operated at temperatures up to 150 K. This was attributed to photogating by the GNR layers that absorbed the MWIR and LWIR radiation, leading to a significant temperature change. These results can potentially contribute toward developing high-performance and broadband IR graphene-based photodetectors. [DOI: 10.1117/1.OE.61.11.115103]

Keywords: graphene; graphene nanoribbon; infrared sensors; photogating; graphene photodetector; field-effect transistor.

Paper 20221086G received Sep. 20, 2022; accepted for publication Oct. 25, 2022; published online Nov. 16, 2022.

1 Introduction

Graphene is an atomically thin carbon sheet with a two-dimensional hexagonal lattice structure.[1,2] It has attracted immense attention in various fields, including electronics,[3] energy storage,[4] biological,[5] spintronics,[6] and photonics[7,8] applications because of its unique electronic and optical properties.[9] In particular, graphene is applicable to photodetectors, which require a broadband photoresponse from the ultraviolet to terahertz regions, high-speed operation, and low fabrication costs.[10–12] Numerous methods, including those employing asymmetric electrodes,[13] plasmonics,[14–17] $p-n$ junctions,[18,19] bolometers,[20,21] photonic cavities,[22–24] waveguides,[25–27] Schottky junctions,[28–30] and photogating,[31–40] have been proposed to enhance the response of graphene-based photodetectors. Among them, photogating is the most promising approach because it can realize the highest performance. Photogating requires the photosensitizers to be present in the vicinity of graphene to produce a voltage change. Various photosensitizers, including h-BN,[39,40] quantum dots,[31] Si,[32,35] InSb,[33,37] and $LiNbO_3$,[34] have been used in the deep-ultraviolet, visible, near-, middle-, and long-wavelength infrared (NIR, MWIR, and LWIR) regions, respectively. In the MWIR and LWIR regions, the applicable photosensitive materials are practically limited to small-bandgap semiconductors such as mercury cadmium telluride and III-V compounds, which are difficult to design, especially for the LWIR region. To address this problem, we have used a graphene nanoribbon (GNR)[41–43] as the photosensitizer for photogating.[44] The GNR is composed of narrow ribbons of graphene, and its energy gaps can be tuned by the number of dimer lines along the width;[45–48] these properties render the GNR promising for use as MWIR and LWIR photosensitizers. In this study, we demonstrate the concept of broadband GNR photogating in graphene photodetectors operated in the MWIR and LWIR regions. The GNR was synthesized through a top-down approach, wherein multiwalled

*Address all correspondence to Shinpei Ogawa, Ogawa.Shimpei@eb.MitsubishiElectric.co.jp

carbon nanotubes were used as the starting materials.[49] The GNR was dispersed on graphene field-effect transistors (GFETs). Raman spectra of the GNR and graphene were obtained, and were used to image the GFET channel. The MWIR and LWIR photoresponses of the devices were evaluated under irradiation at wavelengths of 4.6 and 9.6 μm, respectively.

2 Device Fabrication and Assessment

Figure 1 shows the procedure used to fabricate GFETs with GNR photosensitizers. A 625 μm-thick Si substrate with a 290 nm-thick thermal SiO_2 insulator layer was first prepared [Fig. 1(a)]. The source and drain electrodes were then formed [Fig. 1(b)]. Single-layer graphene was synthesized by chemical vapor deposition (CVD)[50] and transferred onto the electrodes and SiO_2 layer.[51] A soluble GNR with a length > 2 μm and width > 200 nm was obtained from the carbon nanotubes using potassium intercalation.[49] After centrifugation in ethanol to remove aggregation, the GNR was spin-coated on graphene [Fig. 1(c)]. The GNR/GFET channel with a length of 15 μm and width of 5 μm was formed by photolithography and O_2 plasma etching [Fig. 1(d)].

Figure 2 shows a schematic of the GNR/graphene photodetectors. The GNR was coated on the GFET channel. Fibrous GNRs were not aligned in a specific direction on the graphene surface and were stacked randomly. They were adsorbed on the graphene surface, and no peeling was observed after application of the photoresist and rinsing with the organic solvent during the formation of the FET channel. Source-drain bias (V_{sd}) and back-gate (V_{bg}) voltages were applied to the device in a vacuum chamber (GRAIL10-415-4-LV-HT-OP, Nagase Techno-Engineering)

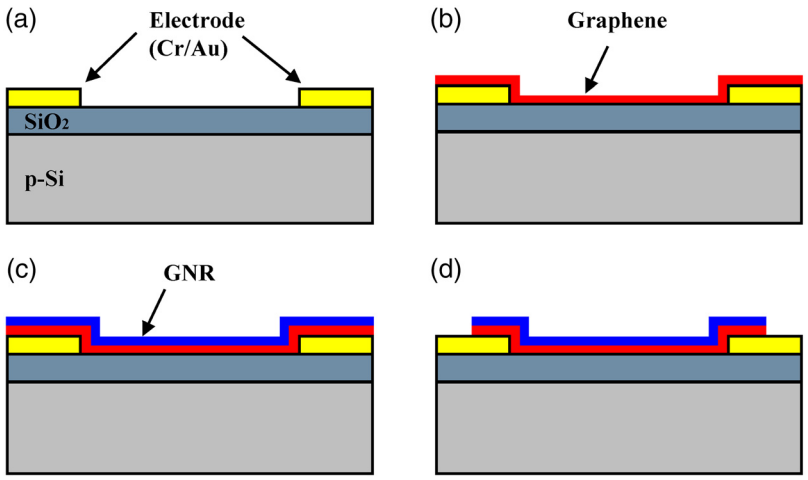

Fig. 1 (a)–(d) Fabrication of GFETs with GNR photosensitizers.

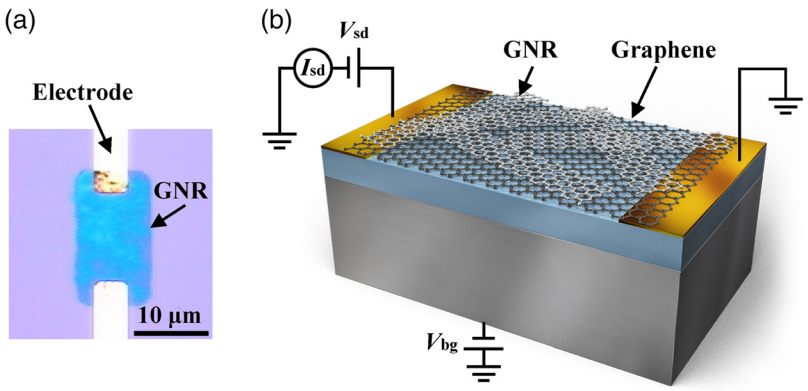

Fig. 2 (a) Light microscopy image and (b) schematic of a GFET with a GNR photosensitizer.

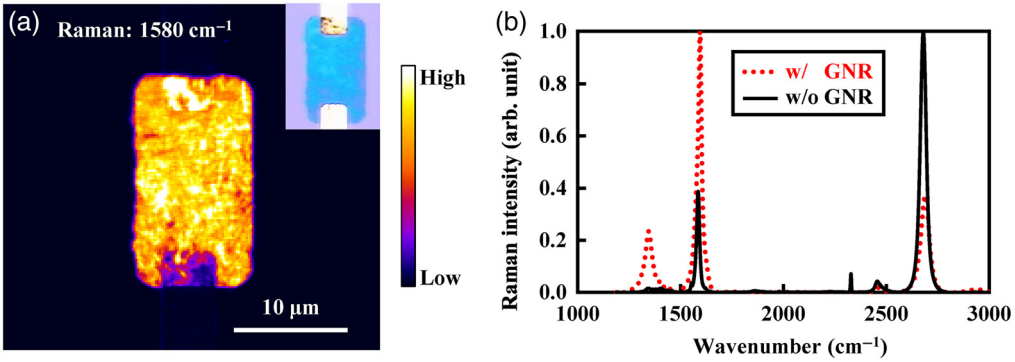

Fig. 3 (a) Raman image at 1580 cm^{-1} of the graphene/GNR photodetectors. Inset: light microscopy image of the device. (b) Raman spectra of the graphene channel with (red, dotted) and without (black, solid) the GNR.

at 10^{-3} Pa and a temperature range of 15–150 K. The current and applied voltage were measured using a device analyzer (B1500A, Keysight).

Figures 3(a) and 3(b) show the light microscopy and Raman spectral mapping images of the GFETs after GNR coating. The light microscopy images and Raman spectral images were obtained using 532 nm laser excitation and Raman microscopy (Raman touch, Nanophoton). The distribution of the fibrous GNRs was confirmed at 1580 cm^{-1}. Figure 3(b) shows the Raman spectra before and after the GNR coating. In addition to the G-mode peak at around 1580 to 1590 cm^{-1} and the 2D-mode peak at around 2680 cm^{-1}, a D-mode peak at around 1340 cm^{-1} derived from carbon lattice defects in the GNR is observed. Although the full width half maximum (FWHM) of the 2D-mode peak was less than 40 cm^{-1} for a single-layer GNR, the device exhibited FWHMs in the range of 2663 to 2771 cm^{-1} corresponding to 48 cm^{-1}, indicating that more than two layers of GNRs were stacked on the graphene channel.

3 Results and Discussion

3.1 *IR Photoresponse*

The graphene channel was exposed to 4.6 and 9.6 μm radiation using a quantum cascade laser with a 2.0 s irradiation cycle (0.8 s on, 1.2 s off) to investigate the MWIR and LWIR photoresponses, respectively. The photoresponse was calculated based on the extent of I_{sd} modulation between illuminated and dark conditions (photocurrent, $I_{ph} = I_{light} - I_{dark}$). The time-dependent current characteristics were measured with a dwell time and measurement resolution of 80 ms and 0.1 fA, respectively. Figures 4(a) and 4(b) show the I_{ph} responses of the device for MWIR

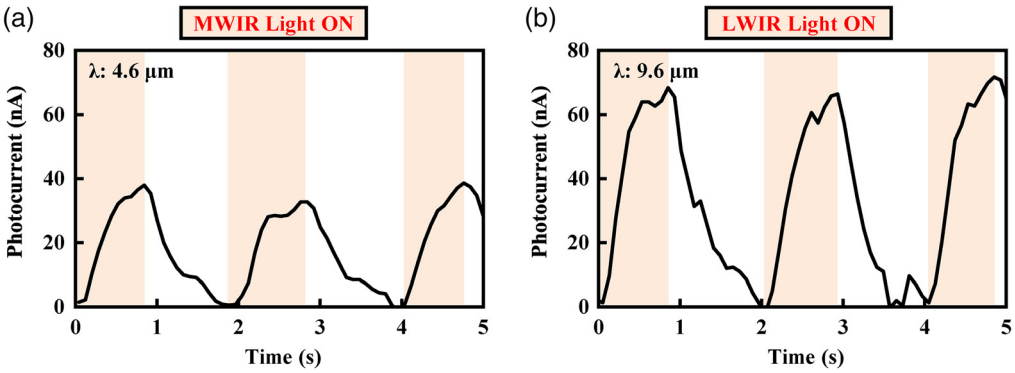

Fig. 4 IR photoresponse of the device under (a) 4.6 μm MWIR light and (b) 9.6 μm LWIR light irradiation.

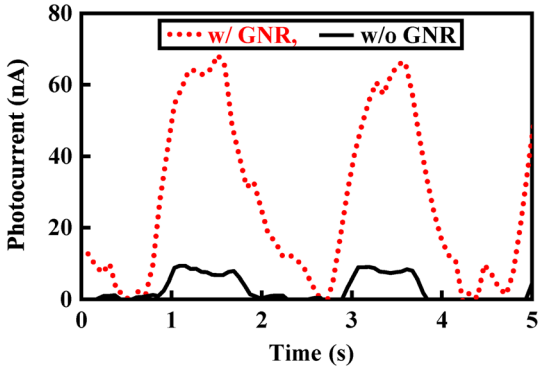

Fig. 5 Comparison of the LWIR photoresponse in the device with (red, dotted) and without (black, solid) the GNR.

and LWIR irradiation, respectively, with $V_{sd} = 0.1$ V and $V_{bg} = 0$ V at 15 K. The device exhibited a definite photoresponse with I_{ph} values of 37 and 65 nA under 4.6 and 9.6 μm light irradiation, respectively. MWIR and LWIR dual-band detection was achieved. The response time was estimated to be 300 to 400 ms.

The response noise and low response time in this device were because of the low carrier mobility and localized distribution of the GNR photosensitizers. The electron field-effect mobility μ_{FE} of the device without GNR photosensitizers was ~6000 $cm^2\,V^{-1}\,s^{-1}$ at the applied V_{bg}, whereas it decreased to 300 $cm^2\,V^{-1}\,s^{-1}$ for that with the GNR photosensitizers. An inhomogeneous distribution of the GNR photosensitizers on the GFET channel causes a temperature gradient on the channel, which can improve its thermal IR photoresponse; however, this may also lead to a decrease in the response time and an increase in the noise. Either the coating conditions can be improved or the stacking direction of each GNR on the GFET channel can be controlled to improve the IR response characteristics by increasing the heat dissipation and transport of thermally excited electrons in the GNRs.

Figure 5 compares the LWIR photoresponses of the devices before and after the GNR coating. The device with the GNR photosensitizers exhibits a clear photoresponse with $I_{ph} = 65$ nA, whereas that without the GNR photosensitizers exhibits $I_{ph} = 9$ nA. Thus, the LWIR photoresponse is enhanced by more than seven times using the GNR photosensitizers.

The photogating effect is primarily attributed to the nature of thermal modulation in the GNR photosensitizers. Under IR irradiation, graphene devices exhibit bolometric[52] and photothermoelectric effects;[53–55] however, the photoresponse from those effects is limited because of their excellent thermal conductivity, which results in a small temperature change. The GNRs increase the absorption of MWIR and LWIR light and change the thermal resistance of the device. Moreover, they modulate the photothermoelectric properties of graphene because of their nonuniformity. The response time of the device with the GNRs is inferior to that of the device without them, suggesting that the main mechanism of response amplification is the enhancement of the bolometric effect by the GNR coating. The GNR coating increases the number of layers of graphene channels on the device more easily than graphene transfer methods, allowing for an improved thermal IR photoresponse.

3.2 *Temperature Dependence of Photogating*

The effect of temperature on the device was assessed. Figure 6(a) shows the LWIR photoresponse of the device at various temperatures. At 150 K, the photogating effect is reduced by the thermal noise of the GNR photosensitizers because of thermally generated carriers, thereby decreasing the LWIR photoresponse. At temperatures higher than 150 K, the LWIR photoresponse of the device is no longer observed. Figure 6(b) shows the temperature dependence of the device responsivity. The LWIR responsivity decreases with increasing temperature. The photogating effect of the GNR photosensitizers is reduced by the decrease in the temperature change during IR irradiation due to low heat dissipation and a reduction of the bolometric effect.

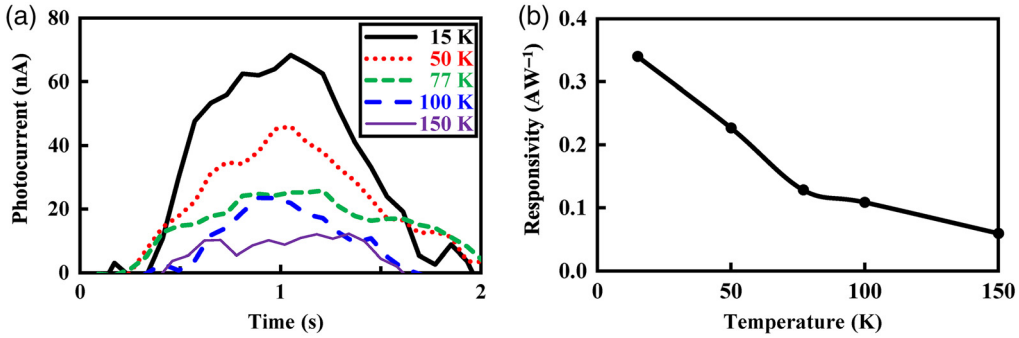

Fig. 6 (a) Photocurrent–time characteristics at various temperatures. (b) Dependence of the responsivity on the device temperature.

The operational temperature range can be further extended by improving the GNR coating conditions and thermal insulation of the GNR/graphene channel region to efficiently maintain the IR response under thermal effects.

4 Conclusion

We proposed GFETs with GNR photosensitizers for broadband IR operation. The GNR was formed on a graphene channel using a solution dispersion method. The photoresponse of the device was measured in the MWIR and LWIR regions. The photoresponse was enhanced by GNR photogating compared with devices without GNR photosensitizers. We expect that the device performance can be further enhanced through optimization of the thickness and density of the GNR layer and improvements to the fabrication process. The results presented here are expected to contribute to the development of high-performance broadband IR photodetectors.

Acknowledgments

This work was supported by Innovative Science and Technology Initiative for Security Grant Number JPJ004596, ATLA, Japan. There are no conflicts to declare.

References

1. K. S. Novoselov et al., "Electric field effect in atomically thin carbon films," *Science* **306**(5696), 666–669 (2004).
2. A. H. Castro Neto et al., "The electronic properties of graphene," *Rev. Mod. Phys.* **81**(1), 109–162 (2009).
3. A. D. Franklin, "Nanomaterials in transistors: From high-performance to thin-film applications," *Science* **349**(6249), aab2750 (2015).
4. F. Bonaccorso et al., "2D materials. Graphene, related two-dimensional crystals, and hybrid systems for energy conversion and storage," *Science* **347**(6217), 1246501 (2015).
5. S. J. Heerema and C. Dekker, "Graphene nanodevices for DNA sequencing," *Nat. Nanotechnol.* **11**(2), 127–136 (2016).
6. W. Han et al., "Graphene spintronics," *Nat. Nanotechnol.* **9**(10), 794–807 (2014).
7. M. Romagnoli et al., "Graphene-based integrated photonics for next-generation datacom and telecom," *Nat. Rev. Mater.* **3**(10), 392–414 (2018).
8. Q. Bao and K. P. Loh, "Graphene photonics, plasmonics, and broadband optoelectronic devices," *ACS Nano* **6**(5), 3677–3694 (2012)
9. F. Bonaccorso et al., "Graphene photonics and optoelectronics," *Nat. Photonics* **4**, 611–622 (2010).
10. F. H. L. Koppens et al., "Photodetectors based on graphene, other two-dimensional materials and hybrid systems," *Nat. Nanotechnol.* **9**(10), 780–793 (2014).

11. T. Low and P. Avouris, "Graphene plasmonics for terahertz to mid-infrared applications," *ACS Nano* **8**(2), 1086–1101 (2014).
12. G. Wang et al., "Two dimensional materials based photodetectors," *Infrared Phys. Technol.* **88**, 149–173 (2018).
13. T. Mueller, F. Xia, and P. Avouris, "Graphene photodetectors for high-speed optical communications," *Nat. Photonics* **4**(5), 297–301 (2010).
14. S. Ogawa, D. Fujisawa, and M. Ueno, "Effect of graphene on plasmonic metasurfaces at infrared wavelengths," *AIP Adv.* **3**(11), 112127 (2013).
15. Y. Yao et al., "High-responsivity mid-infrared graphene detectors with antenna-enhanced photocarrier generation and collection," *Nano Lett.* **14**, 3749–3754 (2014).
16. Z. Fang et al., "Graphene-antenna sandwich photodetector," *Nano Lett.* **12**(7), 3808–3813 (2012).
17. S. Ogawa, S. Fukushima, and M. Shimatani, "Graphene plasmonics in sensor applications: a review," *Sensors* **20**(12), 3563 (2020).
18. N. Liu et al., "Large-area, transparent, and flexible infrared photodetector fabricated using P-N junctions formed by N-doping chemical vapor deposition grown graphene," *Nano Lett.* **14**(7), 3702–3708 (2014).
19. M. Shimatani et al., "Photocurrent enhancement of graphene phototransistors using p–n junction formed by conventional photolithography process," *Jpn. J. Appl. Phys.* **55**(11), 110307 (2016).
20. J. Yan et al., "Dual-gated bilayer graphene hot-electron bolometer," *Nat. Nanotechnol.* **7**(7), 472–478 (2012).
21. A. Blaikie, D. Miller, and B. J. Aleman, "A fast and sensitive room-temperature graphene nanomechanical bolometer," *Nat. Commun.* **10**(1), 4726 (2019).
22. M. Engel et al., "Light–matter interaction in a microcavity-controlled graphene transistor," *Nat. Commun.* **3**, 906 (2012).
23. M. Furchi et al., "Microcavity-integrated graphene photodetector," *Nano Lett.* **12**(6), 2773–2777 (2012).
24. D. K. Efetov et al., "Fast thermal relaxation in cavity-coupled graphene bolometers with a Johnson noise read-out," *Nat. Nanotechnol.* **13**, 797–801 (2018).
25. X. Gan et al., "Chip-integrated ultrafast graphene photodetector with high responsivity," *Nat. Photonics* **7**(11), 883–887 (2013).
26. A. Pospischil et al., "CMOS-compatible graphene photodetector covering all optical communication bands," *Nat. Photonics* **7**(11), 892–896 (2013).
27. X. Wang et al., "High-responsivity graphene/silicon-heterostructure waveguide photodetectors," *Nat. Photonics* **7**(11), 888–891 (2013).
28. A. Di Bartolomeo, "Graphene Schottky diodes: an experimental review of the rectifying graphene/semiconductor heterojunction," *Phys. Rep.* **606**, 1–58 (2016).
29. X. An et al., "Tunable graphene-silicon heterojunctions for ultrasensitive photodetection," *Nano Lett.* **13**(3), 909–916 (2013).
30. M. Casalino et al., "Vertically illuminated, resonant cavity enhanced, graphene–silicon Schottky photodetectors," *ACS Nano* **11**, 10955–10963 (2017).
31. G. Konstantatos et al., "Hybrid graphene-quantum dot phototransistors with ultrahigh gain," *Nat. Nanotechnol.* **7**(6), 363–368 (2012).
32. M. Shimatani et al., "Giant Dirac point shift of graphene phototransistors by doped silicon substrate current," *AIP Adv.* **6**(3), 035113 (2016).
33. S. Fukushima et al., "High responsivity middle-wavelength infrared graphene photodetectors using photo-gating," *Appl. Phys. Lett.* **113**(6), 061102 (2018).
34. M. Shimatani et al., "Enhanced photogating via pyroelectric effect induced by insulator layer for high-responsivity long-wavelength infrared graphene-based photodetectors operating at room temperature," *Appl. Phys. Exp.* **12**(2), 025001 (2019)
35. S. Ogawa et al., "Broadband photoresponse of graphene photodetector from visible to long-wavelength infrared wavelengths," *Opt. Eng.* **58**(5), 057106 (2019).
36. M. Shimatani et al., "High-performance graphene/InSb heterojunction photodetectors for high-resolution mid-infrared image sensors," *Appl. Phys. Lett.* **117**(17), 173102 (2020).

37. S. Fukushima et al., "Photogating for small high-responsivity graphene middle-wavelength infrared photodetectors," *Opt. Eng.* **59**(3), 037101 (2020).
38. S. Fukushima et al., "Carrier density modulation and photocarrier transportation of graphene/InSb heterojunction middle-wavelength infrared photodetectors," *Opt. Eng.* **59**(9), 097101 (2020)
39. S. Fukushima et al., "Graphene-based deep-ultraviolet photodetectors with ultrahigh responsivity using chemical vapor deposition of hexagonal boron nitride to achieve photogating," *Opt. Mater. Express* **12**(5), 2090–2101 (2022).
40. J. E. Thompson, D. Smalley, and M. Ishigami, "Solar-blind ultraviolet photodetectors based on vertical graphene-hexagonal boron nitride heterostructures," *MRS Adv.* **5**(37), 1993–2002 (2020).
41. L. Jiao et al., "Narrow graphene nanoribbons from carbon nanotubes," *Nature* **458**(7240), 877–880 (2009).
42. H. Suzuki et al., "Wafer-scale fabrication and growth dynamics of suspended graphene nanoribbon arrays," *Nat. Commun.* **7**, 11797 (2016).
43. A. Celis et al., "Graphene nanoribbons: fabrication, properties and devices," *J. Phys. D: Appl. Phys.* **49**(14), 143001 (2016).
44. S. Ogawa et al., *Graphene Nanoribbon Photogating for Graphene-based Infrared Photodetectors*, SPIE Press, Bellingham, Washington (2021).
45. N. Merino-Diez et al., "Width-dependent band gap in armchair graphene nanoribbons reveals fermi level pinning on Au(111)," *ACS Nano* **11**(11), 11661–11668 (2017).
46. W. X. Wang et al., "Energy gaps of atomically precise armchair graphene sidewall nanoribbons," *Phys. Rev. B* **93**(24), 241403 (2016).
47. X. H. Zheng et al., "Band gap engineering in armchair-edged graphene nanoribbons by edge dihydrogenation," *Comput. Mater. Sci.* **62**, 93–98 (2012).
48. S. Singh and I. Kaur, "Bandgap engineering in armchair graphene nanoribbon of zigzag-armchair-zigzag based Nano-FET: a DFT investigation," *Phys. E-Low-Dimens. Syst. Nanostruct.* **118**, 113960 (2020).
49. B. Genorio et al., "In situ intercalation replacement and selective functionalization of graphene nanoribbon stacks," *ACS Nano* **6**(5), 4231–4240 (2012).
50. H. Ago et al., "Epitaxial growth and electronic properties of large hexagonal graphene domains on Cu(111) thin film," *Appl. Phys. Exp.* **6**(7), 075101 (2013).
51. J. W. Suk et al., "Transfer of CVD-grown monolayer graphene onto arbitrary substrates," *ACS Nano* **5**(9), 6916 (2011)
52. J. B. Oostinga et al., "Gate-induced insulating state in bilayer graphene devices," *Nat. Mater.* **7**(2), 151–157 (2008).
53. J. C. Song et al., "Hot carrier transport and photocurrent response in graphene," *Nano Lett.* **11**(11), 4688–4692 (2011).
54. N. M. Gabor et al., "Hot carrier-assisted intrinsic photoresponse in graphene," *Science* **334**(6056), 648–652 (2011).
55. D. Sun et al., "Ultrafast hot-carrier-dominated photocurrent in graphene," *Nat. Nanotechnol.* **7**(2), 114–118 (2012).

Shoichiro Fukushima received his BE and ME degrees and PhD from the Graduate School of Engineering Science, Osaka University, Japan, in 2012, 2013, and 2016, respectively. He has been with the Advanced Technology R&D Center, Mitsubishi Electric Corporation, Amagasaki, Japan, since 2016. He works on the development of infrared imaging techniques, including structural analysis, bioimaging, medical/pathological diagnosis, contrast medium, organic/inorganic luminescent phosphors, and infrared sensors. He is currently a head researcher of graphene image sensors.

Masaaki Shimatani received his ME degree from the Interdisciplinary Graduate School of Engineering Science, Kyushu University, Japan, in 2014. He has been with the Advanced Technology R&D Center, Mitsubishi Electric Corporation, Amagasaki, Japan, since 2014. He works on the development of infrared imaging techniques, two-dimensional materials, and plasmonics. He is currently a head researcher of graphene image sensors.

Shinpei Ogawa received his BE and ME degrees and PhD from the Department of Electronic Science and Engineering, Kyoto University, Japan, in 2000, 2002, and 2005, respectively. He has been with the Advanced Technology R&D Center, Mitsubishi Electric Corporation, Amagasaki, Japan, since 2005. He is currently a chief researcher in the department of two-dimensional materials, metamaterials, and nanophotonics.